SMO applied to contact layers at the 32 nm node and below with consideration of MEEF and MRC

Te-Hung Wu*[a], Robert Sinn[b], Bob Gleason[b]
[a]SYS_LSI Division, Samsung Electronic Co., Ltd.
[b]Luminescent Technologies, Inc., Palo Alto CA

ABSTRACT

An illuminator and mask patterns were optimized (SMO) to minimize CD variation of a set of contact patterns selected from logic layouts and an array of SRAM cells. MEEF and defocus characteristics of the target patterns were modeled as functions of constraints on minimum mask features and spaces (MRC). This process was then repeated after linearly shrinking the input patterns by 10%. Common statistical measures of CD control worsen as MRC becomes more restrictive, but these are weak indicators compared to behavior at points in the image that exhibit high MEEF or low depth of focus. SMO solutions for minimum MEEF and maximum depth of focus are different, so some compromise is necessary. By including exposure time among the variables to be optimized, some control over local mask bias is made available to minimize MEEF and loss of litho quality due to MRC.

Keywords: Source-mask optimization, MEEF, MRC

1. INTRODUCTION

The objective behind optimization of masks and illuminators is to produce images with high contrast, large depth of focus, and low MEEF. Much of the earliest work in this field concentrated on optimizing contrast and depth of focus, with the underlying assumption that higher contrast would promote lower MEEF. Later work showed this assumption to be invalid for some patterns, particularly when the optimized mask solutions contained small SRAFs.[1] It is easy to understand this qualitatively. As SRAFs get smaller, the proportional changes of their areas are greater for a specified mask bias. The proportional changes in the quantity of light that they transmit (clear SRAF) or block (opaque SRAF) track their areas. If an SRAF is small enough, the change of intensity with mask bias overcomes the benefit of higher contrast, so MEEF can get worse even as contrast continues to rise. To account for this, the optimization algorithm must include image conditions with mask bias in the objective cost function to be minimized.

In addition to controlling the compromise between MEEF and the combination of contrast and depth of focus, the optimization algorithm must meet constraints on minimum and maximum SRAF sizes. These arise from two considerations: the wafer image must be free of side-lobes, and the mask pattern must meet MRC constraints. The constraints interact, and can produce discontinuities in the solution. For example, consider a layout for which an unconstrained optimization algorithm yields an SRAF that is smaller than allowed by MRC. The algorithm can proceed in one of two ways: enlarge the SRAF to make it pass MRC, or eliminate it completely. In cases for which the enlarged SRAF would create a side lobe, the algorithm must eliminate it. When an SRAF is eliminated to pass MRC or side lobe constraints, contrast and depth of focus will generally be worse, but MEEF might move in either direction. Small SRAFs that must be enlarged or eliminated are not the only ones affected by MRC. SRAFs of any size that are not parallel to the x or y axes must be approximated by a staircase pattern. Minimum segment lengths and corner-to-corner distance checks determine how well a staircase can approximate an ideal SRAF. Expected behavior of images is similar to that in the discussion of small SRAFs. Closer approximations to ideal SRAFs should yield better contrast and depth of focus, but MEEF could go in either direction, because the segmentation length determines the perimeter-to-area ratio that controls sensitivity to mask bias.

The results reported here cover a set of logic clips and an SRAM cell. It is important to note that MEEF and depth of focus are far from constant across a typical logic layout. MEEF and depth of focus commonly vary by factors of two or three at different locations within a clip that is only 1000 nm along each edge. Also, eliminating a small SRAF to improve MEEF or pass MRC only affects image edges within a radius of a few hundreds of nanometers of it. These two considerations imply that averages of image properties are not sensitive indicators for the items of interest in this study.

It is necessary to examine maps of MEEF and focal deviation along with their corresponding mask patterns to understand causes and effects.

2. TARGET PATTERNS

Layout targets included eight clips selected from the contact layer of a logic layout, and an SRAM cell. These appear in Figure 1. Other than in the SRAM cell, all of the contacts are approximately square, with sides in the range of 60 nm to 75 nm, and spaces down to 37 nm. The SRAM cell contains some elongated contacts with jogs in the longer edges. A second SMO run used the same patterns, but modified by a linear shrink of 10%. The patterns were chosen to include a mix of irregular contact placements and repeating arrays, guided by experience in which types of layouts are most likely to pose challenges regarding MEEF or depth of focus.

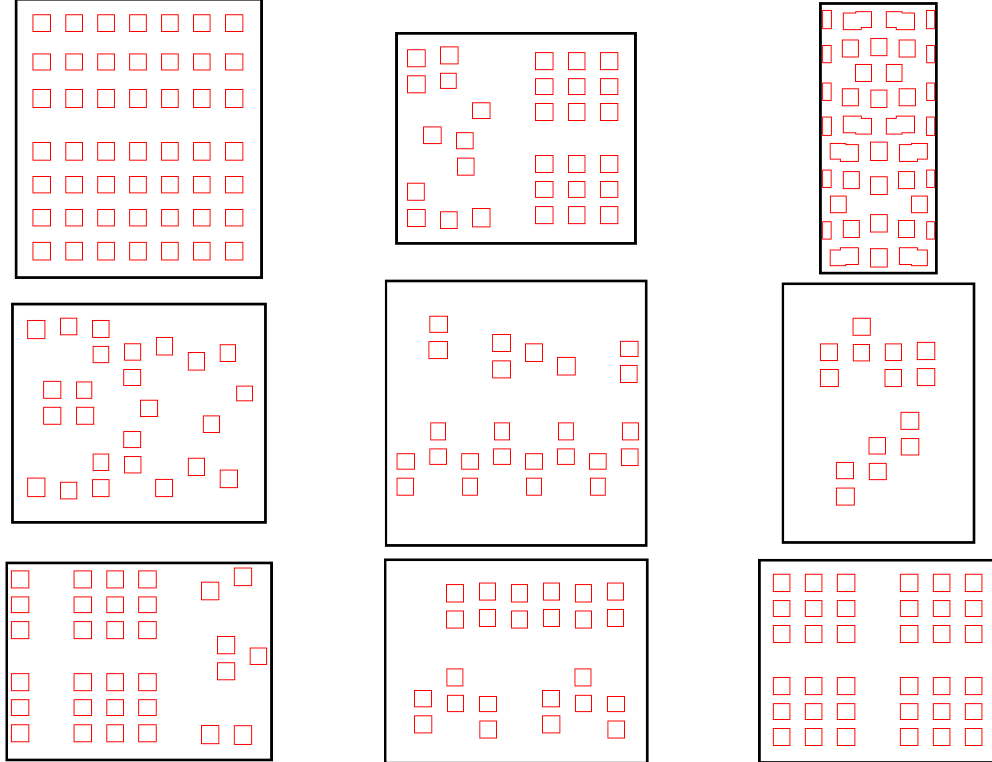

Figure 1. Data clips used for SMO. The SRAM cell is in the upper right corner.

Because the clips are considered to be small extractions from a large design, no additional empty space was added to treat the targets at the edges as if they were isolated on one side. Each of the nine patterns in Figure 1 is tiled horizontally and vertically to create infinite arrays. In the case of the SRAM cell, this completes the partial contacts that are cut by the vertical edges of the unit cell.

3. SMO METHOD

The illuminators were represented as a superposition of dipole and quadrupole sections of an annulus. Figure 2 contains an example comprising a pair of dipoles, a quadrupole, and a disk, and shows the radii and angles that the SMO algorithm optimized. The intensity of each dipole, quadrupole, or disk was also allowed to vary. In total, fifteen variables were used to describe the illuminators, and were available to the SMO algorithm for optimization. Constraints on the variables confined the illuminator to the pupil, and forced it to have specified symmetry. In this case, the illuminator was forced to be invariant under reflections about the x and y axes, which is consistent with the symmetry of the tiled SRAM pattern. Explicit symmetry enforcement is necessary when using samples of real random layouts in the optimization. For example, if each layout rule applies to both x and y directions, the optimum illuminator should be invariant under 90-

degree rotations, although none of the sample clips that appear in Figure 1 exhibit this property. Another reason to use constraints in this representation of the illuminator is to ensure that it can be manufactured and meet specifications for the exposure system on which it is intended to be used. The discussion of the illuminator for the shrunk targets provides an example of this.

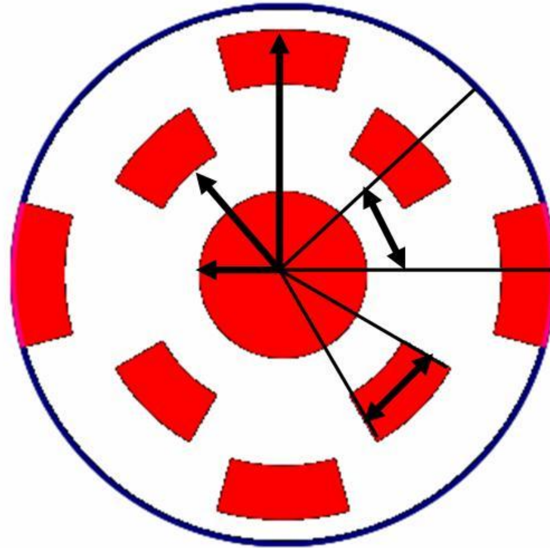

Figure 2. Representation of the illuminator and some geometric variables in the optimization

The method used to optimize the illuminator involves an algorithm that does not require explicit computation of a gradient, avoiding errors and instability associated with numerical differentiation of noisy functions.[2] Because the algorithm starts with a number of illuminators that exceeds the dimension of the space to be searched, it is less likely to get stuck in an unfavorable local minimum than other algorithms using single starting points. For each trial illuminator in the search, masks for each of the target clips are optimized using methods that have been published elsewhere.[3] The objective cost function minimized in the optimization included edge placement errors under conditions of nominal exposure, defocus of 50 nm, and mask bias of ± 0.5 nm (wafer scale). Side lobes were also checked at 5% over exposure. Other than the need to meet MRC specifications, mask solutions were not constrained to meet requirements for simplicity or shot count. Several other publications have addressed the important compromises between litho quality and mask complexity.[4] This is not repeated here because there is no consensus on what amount of mask complexity is tolerable, and adding constraints on complexity might obscure the relation of MRC to SMO.

Freedom to set exposure time is useful to lower MEEF or minimize litho problems related to MRC. To understand this qualitatively, first consider a large array of contacts or lines and spaces that can be discussed in terms of exposure and mask bias. Features can be printed on target over a certain range of exposure times if corresponding changes can be made in mask bias. Although each combination of exposure time and mask bias can put nominal images on target, MEEF and depth of focus are not the same. Figure 3 shows a typical trend in which depth of focus is better when the mask patterns are small, but MEEF is best when they are large. Large MEEF for a small aperture is easy to understand because the percentage of its area and the light it transmits change more for a given mask bias than those of a large aperture.

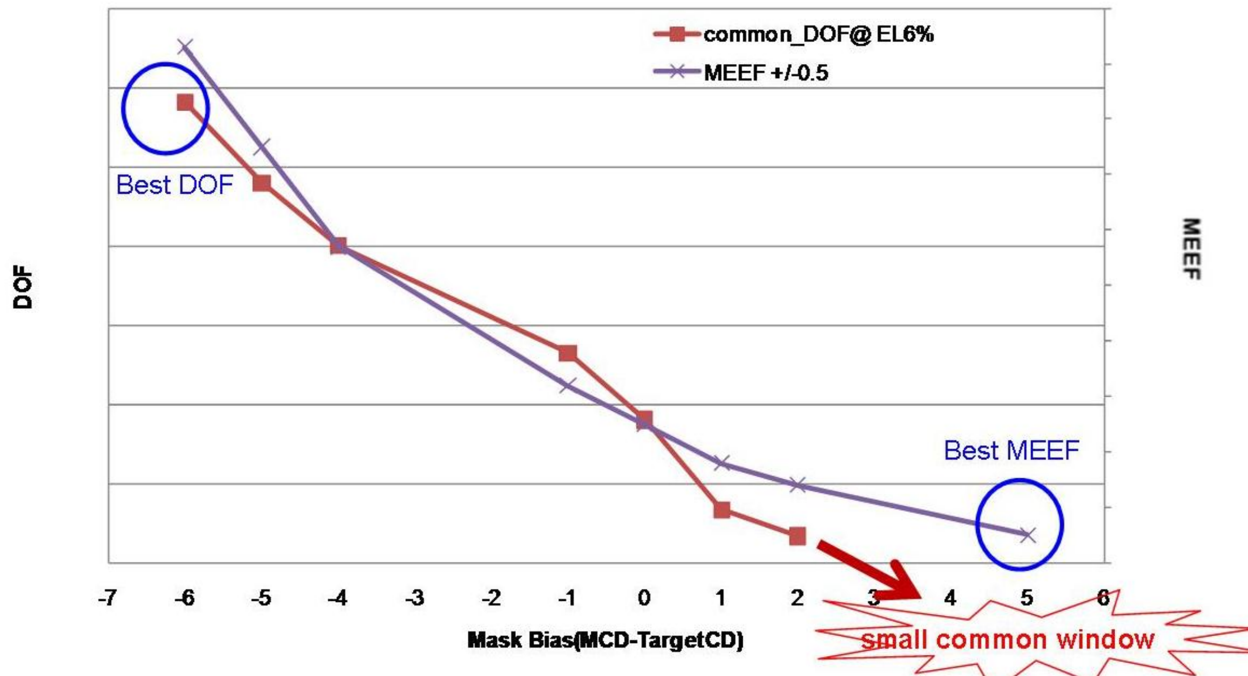

Figure 3. Trends of depth of focus and MEEF with mask bias

The work reported here extends the concepts shown in Figure 3 to more general patterns, for which applying a constant mask bias would throw many of the images off target. This was done for the targets in Figure 1 by changing the exposure time, which is one of the input variables to the mask optimization. For longer exposure times the optimized mask apertures are smaller, and vice versa. This effectively adjusts the bias of each edge relative to the target in such a way to keep all of the images on target. Because MEEF and depth of focus are not optimum at the same bias, the relative weights of their corresponding image terms in the cost function must be set to balance their contributions to total CD errors. The degree to which MRC affects litho performance can also be strongly influenced by mask bias. The minimum features of the targets in Figure 1 are spaces between contacts, so MRC creates more problems as the mask apertures get larger. To deal with these issues, exposure time was included in the initial SMO process. It and the illuminator were then fixed, and masks re-optimized with different MRC constraints to determine how MRC affected litho characteristics.

4. RESULTS

All solutions were computed for 193 nm immersion optics with a numerical aperture of 1.35 and x-y polarized illumination. Illuminators were constrained to be invariant under reflections about the x and y axes, but 90-degree rotational symmetry was not required. Illuminators for the targets of Figure 1, without and with a 10% shrink, appear in Figure 4. Differences between the two illuminators are partly due to the shrink, and partly due to application of a minimum width constraint to each aperture of the illuminator on the right side of the figure. The constraint inhibits the optimization algorithm from converging to a solution that includes the narrow sectors of the ring that joins pairs of poles on the right. Four poles are common to both solutions, and move toward the circumference of the pupil as the patterns are shrunk.

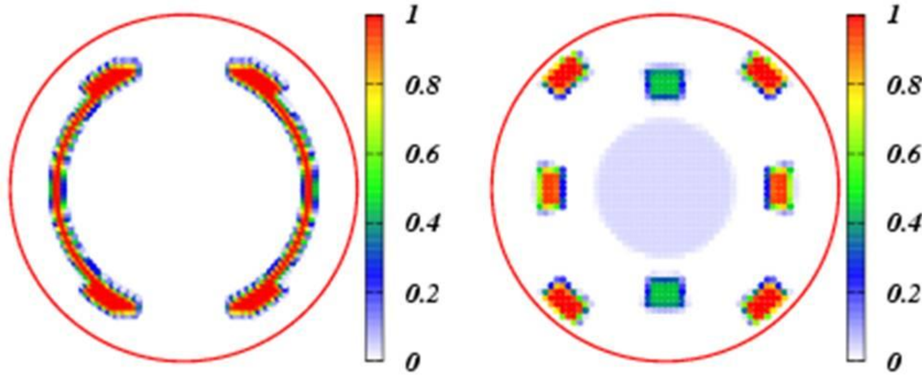

Figure 4. Illuminators optimized for targets in Figure 1 without (left) and with (right) a linear shrink of 10%. The minimum widths of the apertures of the illuminator on the right were also constrained to be 10% of the radius of the pupil.

Figures 5 and 6 show average MEEF and defocus behavior, plotted against the minimum line and space MRC values. Throughout this paper, all dimensions are stated at wafer scale, so the 10 – 26 nm range corresponds to 40 – 104 nm on the mask. The width of the focus band in the plots is the distance between the images at best focus and 50 nm defocus, all at nominal exposure. Note the difference in the vertical scales for the patterns with and without the 10% shrink; the shrunk patterns having higher MEEF and more defocus variation, as expected. The variation of average MEEF and defocus band width with MRC limits shown in these figures is on the order of 10% or less. To see behavior that really matters, it is necessary to consider specific locations on the clips.

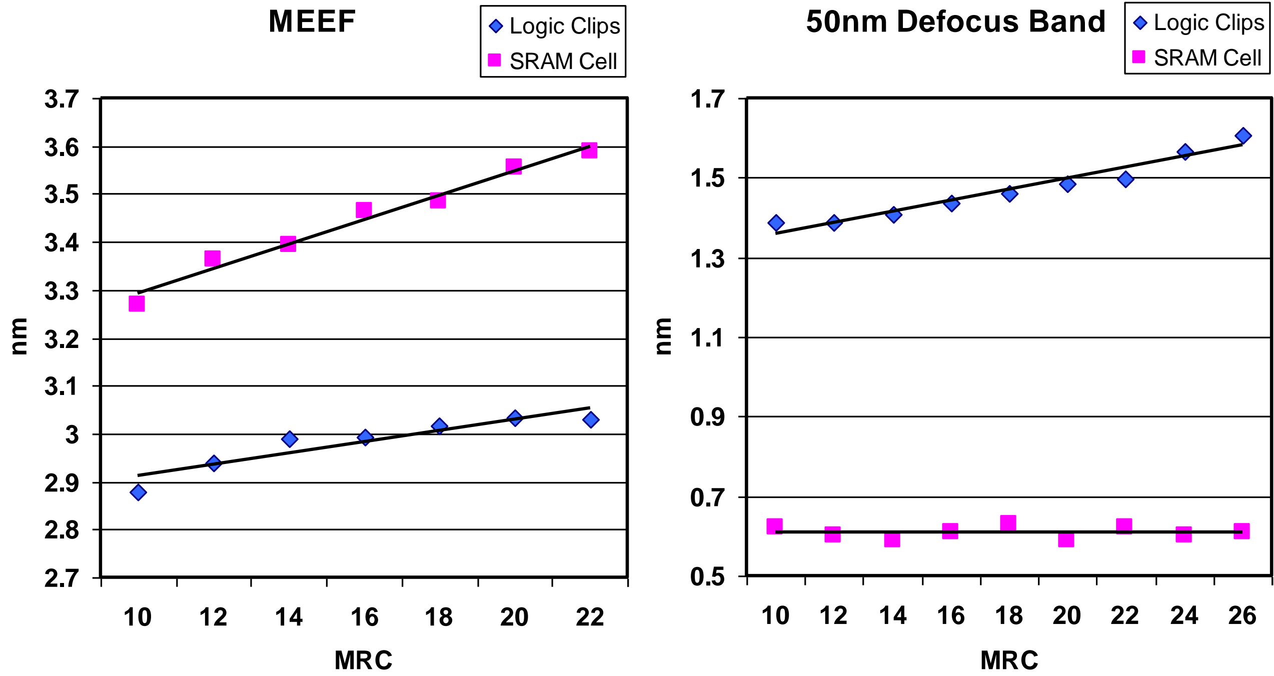

Figure 5. Average MEEF and distance between images at nominal focus and 50 nm defocus. The nm indicator on the MEEF plot shows the image band width between ± 0.5 nm (wafer scale).

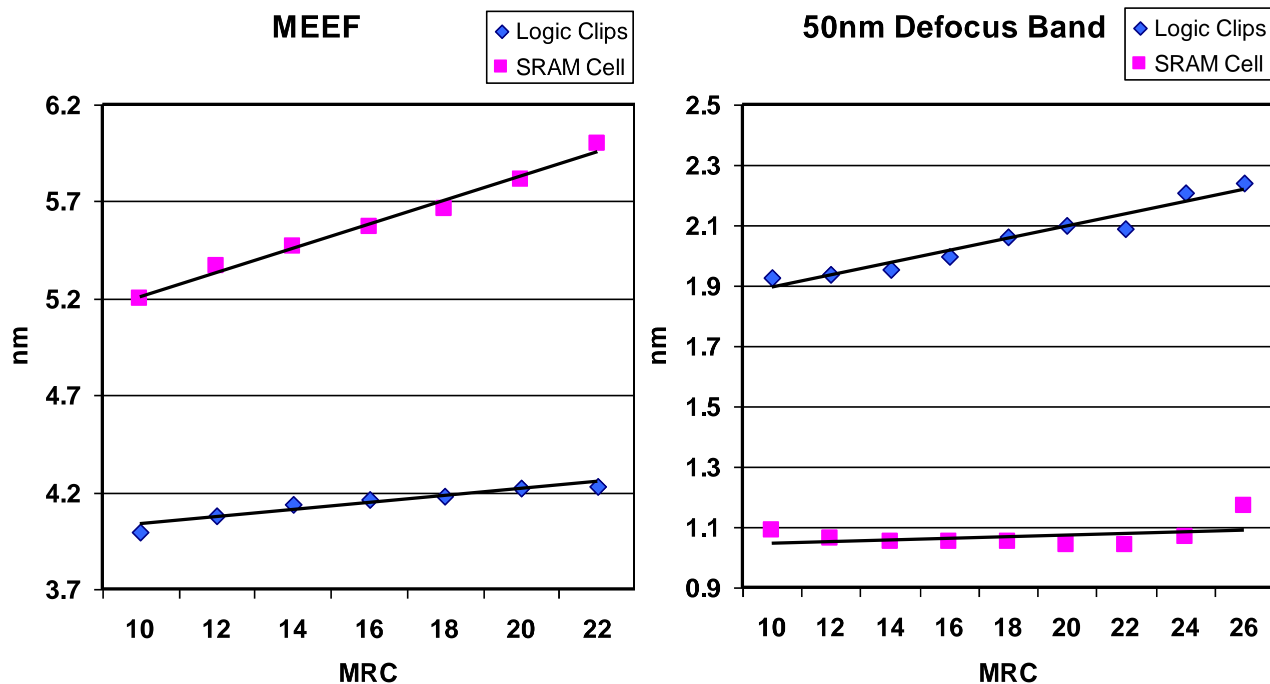

Figure 6. Average MEEF and distance between images at nominal focus and 50 nm defocus for target patterns shrunk by 10%.

Results for one of the logic clips in the study appear in Figures 7, 8, and 9. Each figure contains results for low (least restrictive) MRC limits on the left, and high MRC limits on the right. Because they are the smallest patterns in the solution, SRAFs are most sensitive to MRC. Comparing the two sides of Figure 7 shows that some of the SRAFs have been enlarged, and some eliminated to meet the more restrictive MRC limits on the right. The horizontal SRAF that separates the two blocks of nine contacts has been split into two on the right because the narrowest part of it cannot be expanded to 22 nm without violating side-lobe conditions specified in the optimization. Coarser segment lengths required for the solution with higher MRC limits have reduced curvature of the SRAF patterns in some locations.

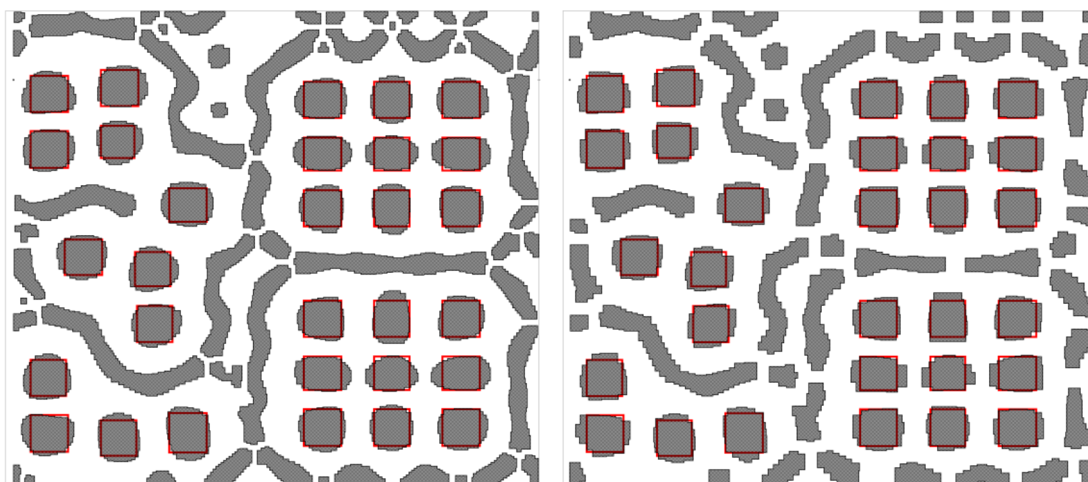

Figure 7. Mask (gray) and target (red) for one of the logic clips in the optimization. The mask on the left is optimized for a MRC constraint of 10 nm (wafer scale), the one on the right for 22 nm.

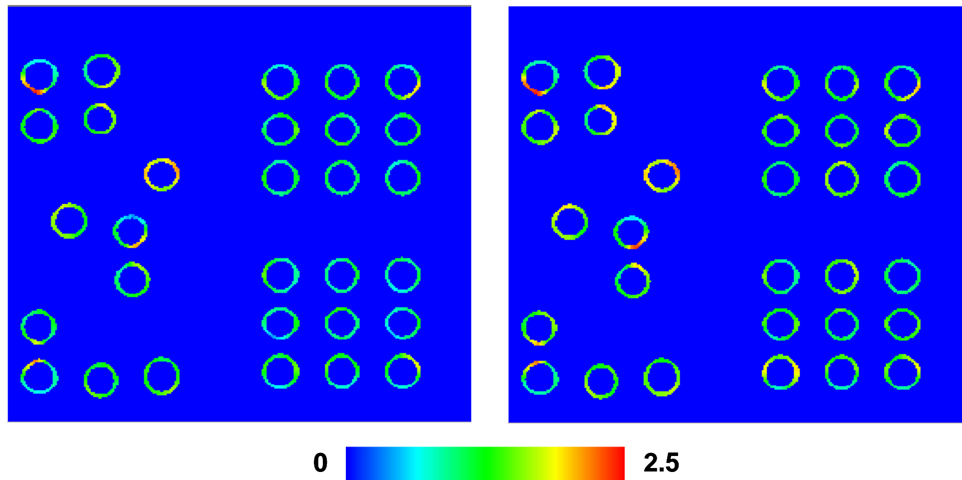

Figure 8. Difference map for image contours under nominal and 50 nm defocus conditions for the masks and target patterns shown in Figure 7. The color scale indicates the width of the defocus band in nanometers. The left figure is for 10 nm MRC, the right for 22 nm.

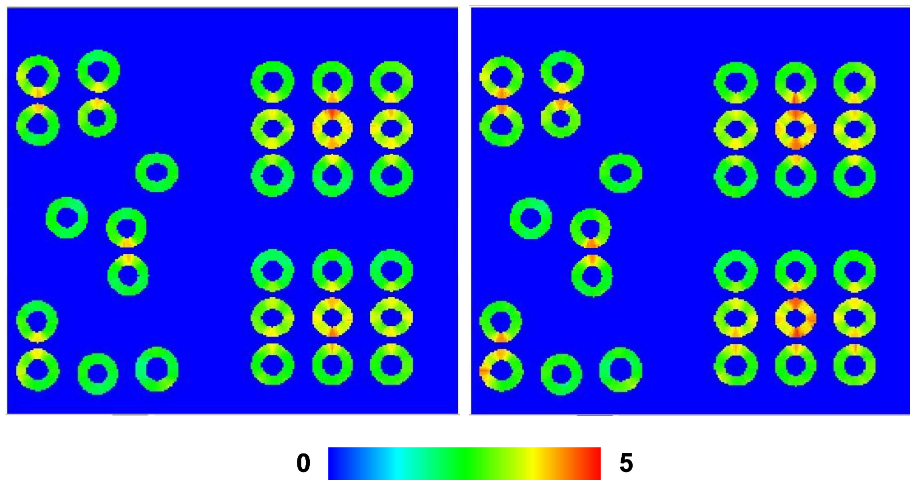

Figure 9. MEEF map for image contours for the masks and target patterns shown in Figure 7. The color scale indicates MEEF. The left figure is for 10 nm MRC, the right for 22 nm.

Width of the defocus band and MEEF vary with position in the clip from about the center of the color scale to its maximum. At some locations there is little difference in performance for the two MRC limits, for example depth of focus at the centers of the blocks of nine contacts and MEEF along their edges show little dependence on MRC. Changes in depth of focus and MEEF at minimum spaces between pairs of contacts are more significant. The defocus band is larger for the contacts nearest the location at which the horizontal SRAF had to be broken to pass 22 nm MRC. MEEF at the centers of the blocks of nine contacts is also sensitive to MRC limits. Numerically, widths of the defocus bands and MEEF at selected locations increase by about 50% as MRC limits change from 10 nm to 22 nm. This is about five times the variation of the mean statistics in Figures 5 and 6.

This clip shows characteristics of MEEF and depth of focus that were common to many others. Interior regions of blocks of contacts mainly suffer from high MEEF, but have good depth of focus. Contacts at the edges of the blocks have better MEEF, but less depth of focus. Pairs of contacts at minimum spacing suffer from both high MEEF and low depth of focus. These observations show the importance of selecting the right patterns for SMO. As noted in the discussion of Figure 3, SMO generally involves a compromise between MEEF and depth of focus. If the input patterns for SMO are repeating arrays for which worst defocus characteristics and worst MEEF occur at different locations, each may be

optimized more or less independently of the other, so the optimization algorithm may be unaware that compromise is necessary. This problem does not occur if the input patterns contain real design clips for which highest MEEF and worst depth of focus can occur at the same place.

The same observations explain why the SRAM clip behaved so differently than the logic clips in Figures 5 and 6.

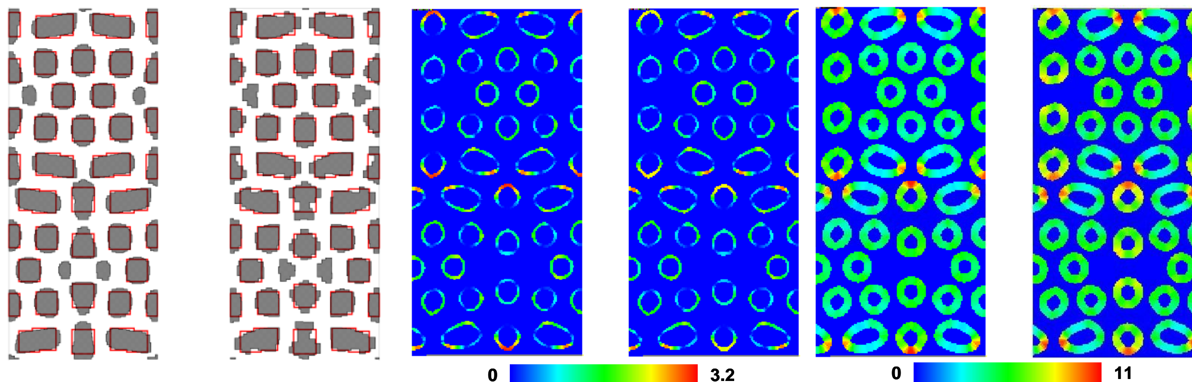

Figure 10. SRAM masks, defocus bands, and MEEF map for input with 10% linear shrink. Two versions correspond to MRC limits of 10 nm (left), and 22 nm (right).

Figure 10 shows the same plots as for the logic clip in Figures 7, 8, and 9. Due to the high density of the SRAM, only four small SRAFs appear in the solution, and they are not adjacent to the high MEEF points that limit the litho performance of this layout. The SRAM layout behaves qualitatively much like the center contacts within the 3x3 blocks of the logic clip; MEEF is much worse than depth of focus, consistent with the results shown in Figures 5 and 6. The additional information in Figure 10 is that highest MEEF and (less importantly) worst depth of focus occur near the ends of the rectangular contacts. These were the highest MEEFs shown by any of the patterns in the study. Although MEEF at other points in the SRAM cell became worse with more restrictive MRC, the worst points changed very little.

5. CONCLUSIONS

Because SMO involves compromises between MEEF and depth of focus, weights of their terms in the optimization must be assigned carefully to produce desired results. If exposure time is one of the variables to be optimized, it may be used to effectively change local mask bias, reducing MEEF, and minimizing effects of MRC on the solution. MEEF and CD variation with defocus change significantly with location in the image, so mean statistics are not adequate to judge the quality of SMO solutions. Maps that show local MEEF and defocus characteristics are more useful. Repeating arrays generally show high MEEF in their interiors and low depth of focus along their perimeters, but for random logic layouts, high MEEF and low depth of focus can occur at the same place. This should be considered when selecting the input patterns for SMO. MRC limits must continue to shrink along with CDs to achieve acceptable MEEF and depth of focus.

REFERENCES

[1] L. Pang, G. Xiao, V. Tolani, P. Hu, T. Cecil, T. Dam, K. Baik, B. Gleason "Considering MEEF in Inverse Lithography Technology (ILT) and Source Mask Optimization (SMO)" Proc. of SPIE, Vol. 7122, 71221W, 2008

[2] V. Torczon "Multidirectional Search" Ph.D. Thesis, Rice University, 1989

[3] D. Abrams, L. Pang "Fast Inverse Lithography Technology" Proc. of SPIE, Vol. 6154, 64511J, 2006.

[4] B. Kim, S. Suh, S. Woo, H. Cho, G. Xiao, D. Son, D. Irby, D. Kim, K. Baik "Inverse lithography (ILT) mask manufacturability for full-chip device" Proc. SPIE, Vol. 7488, 748812, 2009